ChemComm

COMMUNICATION

View Article Online
View Journal

Cite this: DOI: 10.1039/c7cc01480e

Received 24th February 2017,
Accepted 16th March 2017

DOI: 10.1039/c7cc01480e

rsc.li/chemcomm

Chemoproteomics-enabled covalent ligand screen reveals a cysteine hotspot in reticulon 4 that impairs ER morphology and cancer pathogenicity†

L. A. Bateman,‡[ab] T. B. Nguyen,‡[b] A. M. Roberts,‡[a] D. K. Miyamoto,[a] W.-M. Ku,[a] T. R. Huffman,[a] Y. Petri,[a] M. J. Heslin,[c] C. M. Contreras,[c] C. F. Skibola,[c] J. A. Olzmann*[b] and D. K. Nomura *[ab]

Chemical genetics has arisen as a powerful approach for identifying novel anti-cancer agents. However, a major bottleneck of this approach is identifying the targets of lead compounds that arise from screens. Here, we coupled the synthesis and screening of fragment-based cysteine-reactive covalent ligands with activity-based protein profiling (ABPP) chemoproteomic approaches to identify compounds that impair colorectal cancer pathogenicity and map the druggable hotspots targeted by these hits. Through this coupled approach, we discovered a cysteine-reactive acrylamide DKM 3-30 that significantly impaired colorectal cancer cell pathogenicity through targeting C1101 on reticulon 4 (RTN4). While little is known about the role of RTN4 in colorectal cancer, this protein has been established as a critical mediator of endoplasmic reticulum tubular network formation. We show here that covalent modification of C1101 on RTN4 by DKM 3-30 or genetic knockdown of RTN4 impairs endoplasmic reticulum and nuclear envelope morphology as well as colorectal cancer pathogenicity. We thus put forth RTN4 as a potential novel colorectal cancer therapeutic target and reveal a unique druggable hotspot within RTN4 that can be targeted by covalent ligands to impair colorectal cancer pathogenicity. Our results underscore the utility of coupling the screening of fragment-based covalent ligands with isoTOP-ABPP platforms for mining the proteome for novel druggable nodes that can be targeted for cancer therapy.

Traditional strategies for cancer target discovery often involve searching for proteins or genes that are dysregulated or mutated in tumors, which may miss promising therapeutic targets that may not necessarily be changing in expression or activity. Screening chemical libraries for anti-cancer small-molecules using chemical genetics strategies has arisen as a powerful complementary approach to traditional target discovery approaches for mining druggable nodes that can be pharmacologically interrogated in cancer.[1,2] However, a major challenge of chemical genetics is identifying the targets of leads that arise from screens. Oftentimes, lead compounds must be derivatized to either bear bioorthogonal and/or photoaffinity handles or conjugated to beads to facilitate chemoproteomic target identification.[2] However, these approaches frequently require additional synthetic efforts to make analogs of the lead molecule thereby hindering or preventing target identification.

Here, we have generated a library of 75 fragment-based cysteine-reactive covalent ligands and coupled the screening of this library with an isotopic tandem orthogonal proteolysis-enabled activity-based protein profiling (isoTOP-ABPP) platform to rapidly identify covalent ligands that impair colorectal cancer pathogenicity and to map the druggable hotspots targeted by these hits (Fig. 1A). IsoTOP-ABPP uses reactivity-based chemical probes to map proteome-wide reactive, functional, and ligandable hotspots. When used in a competitive manner, covalent small-molecules can be competed against the binding of their corresponding reactivity-based probes to rapidly identify the targets of these molecules.[3–5] In this study, upon identifying a cysteine-reactive lead fragment, the lead molecules can compete with a broad cysteine-reactive probe to subsequently identify its targets and the specific sites of labelling.

There are several advantages to this combined approach. Our library already introduces specific covalent interactions through the incorporation of cysteine-reactive acrylamide and chloroacetamide warheads, thus avoiding the necessity for introducing photoaffinity handles for target identification. Recent studies by Backus *et al.* have shown that the reactivity of these scaffolds can be tempered and made to confer substantial selectivity through appending small-molecular weight fragments.[4] Also, because these compounds are small molecular weight fragment-based covalent ligands, they can sample more macromolecular protein space and enable interrogation of more druggable nodes, a notion explored by many pharmaceutical companies with fragment-based ligand discovery.[6]

We screened our cysteine-reactive ligand library of acrylamides and chloroacetamides to identify compounds that impair colorectal cancer cell survival and proliferation in the highly metastatic and tumorigenic SW620 colorectal cancer cell line (Fig. 1B and Table S1, ESI†). We identified a lead acrylamide DKM 3-30 as the top hit from

[a] *Departments of Chemistry and Molecular and Cell Biology, University of California, Berkeley, Berkeley, CA 94720, USA. E-mail: dnomura@berkeley.edu*
[b] *Department of Nutritional Sciences and Toxicology, University of California, Berkeley, Berkeley, CA 94720, USA. E-mail: olzmann@berkeley.edu*
[c] *The University of Alabama at Birmingham, Birmingham, AL 35233, USA*
† Electronic supplementary information (ESI) available. See DOI: 10.1039/c7cc01480e
‡ These authors contributed equally to this paper.

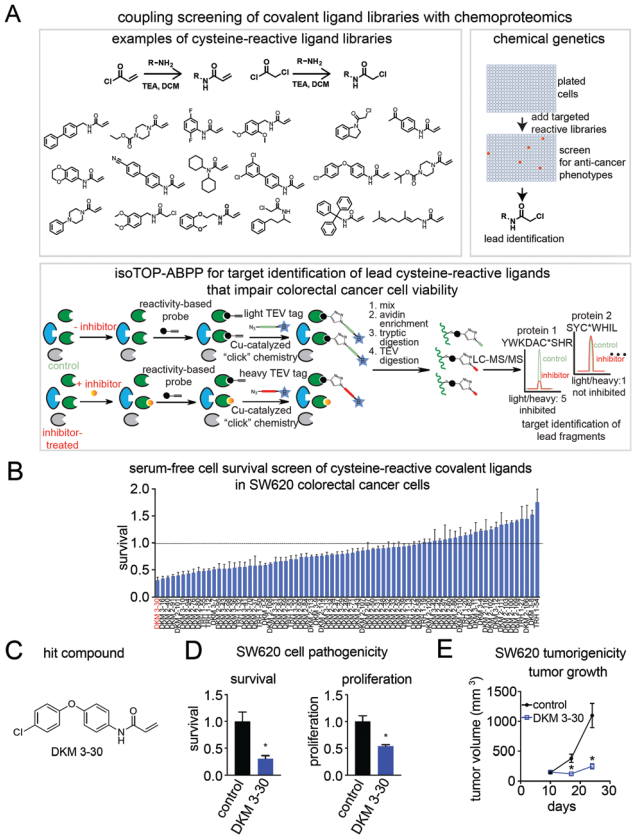

Fig. 1 Coupling screening of cysteine-reactive covalent ligands with isoTOP-ABPP to identify anti-cancer compounds and druggable hotspots for colorectal cancer. (A) We screened a library of cysteine-reactive fragment-based covalent ligands in colorectal cancer cells to identify compounds that impair colorectal cancer pathogenicity and used isoTOP-ABPP to identify the druggable hotspots targeted by hits. (B) We screened a cysteine-reactive fragment library consisting of acrylamides and chloroacetamides in SW620 colorectal cancer cells (50 μM) to identify any leads that significantly impaired SW620 serum-free cell survival. (C and D) Shown is the structure of the lead covalent ligand DKM 3-30 (C) that significantly ($p < 0.05$) impaired SW620 cell survival and proliferation (D). (E) SW620 tumor xenograft growth in immune-deficient SCID mice. Mice were subcutaneously injected with SW620 cells to initiate the tumor xenograft study and treatments of mice were initiated with vehicle or DKM 3-30 (50 mg kg^{-1} ip, once per day) ten days post-initiation of the xenograft study. Data in (B, D and E) are presented as mean ± sem, n = 3–8 per group. Significance expressed as *$p < 0.05$ compared to vehicle-treated controls.

this screen which significantly impaired both serum-free cell survival and proliferation in SW620 colorectal cancer cells (Fig. 1C and D). We further showed that SW620 colorectal tumor xenograft growth was significantly impaired upon *in vivo* treatment of mice with DKM 3-30, started 10 days after the initiation of the xenograft, without any changes in body weight or any signs of overt toxicity (Fig. 1E and Fig. S1, ESI†). Taken together, our data indicated that DKM 3-30 significantly impaired SW620 colorectal cancer pathogenicity.

We next performed isoTOP-ABPP studies to identify the direct targets of these lead compounds. We competed either vehicle or DKM 3-30 against labeling of SW620 proteomes with a broad cysteine-reactive probe, iodoacetamide-alkyne (IAyne), followed by appending probe-labeled proteins with a biotin-azide tag bearing a TEV protease recognition site and an isotopically light (for vehicle-treated) or heavy (for fragment-treated) tags *via* copper catalyzed azide–alkyne cycloaddition (CuAAC).[4,7] We then combined control and treated proteomes in a 1:1 ratio, enriched probe-labeled proteins with avidin, and digested proteomes with trypsin. Avidin-enriched probe-modified tryptic peptides were released by TEV protease digestion for subsequent quantitative proteomic analysis. Through these studies, we identified the top hit for DKM 3-30 as C1101 in reticulon 4 (RTN4, Uniprot ID Q9NQC3-1) with a light to heavy ratio of 3.0 (Fig. 2A and Table S2, ESI†). We further validated this hit by competing DKM 3-30 against IAyne labeling of pure human RTN4 protein using gel-based ABPP methods (Fig. 2A).

To determine the relevance of RTN4 in colorectal cancer, we performed isoTOP-ABPP analysis to quantitatively map proteome-wide reactivity of cysteines in pooled primary human colorectal tumors through comparative ratiometric analysis of IAyne labeling

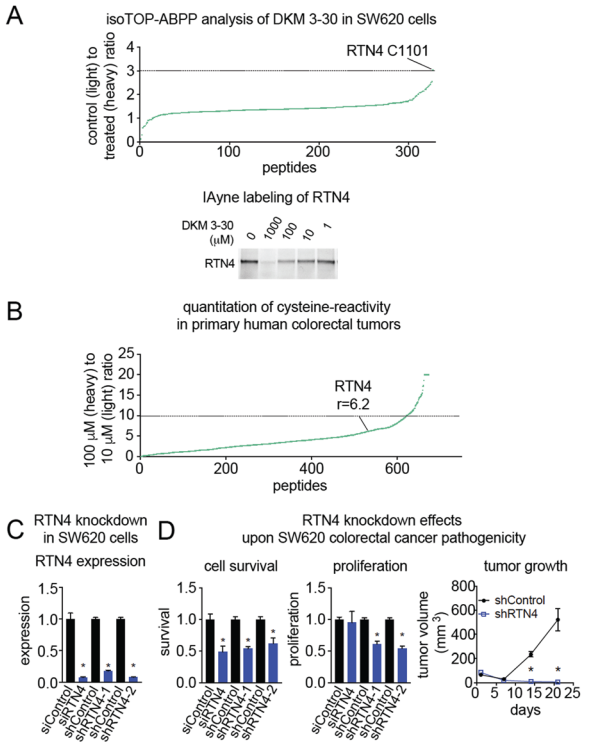

Fig. 2 DKM 3-30 targets C1101 on RTN4. (A) IsoTOP-ABPP analysis of DKM 3-30 in SW620 colorectal cancer cells. SW620 proteomes were pre-treated with DMSO or DKM 3-30 (50 μM) prior to labeling proteomes with IAyne and isoTOP-ABPP analysis. Shown are mean light to heavy ratios for those probe-modified peptides identified in at least 2 out of 3 biological replicates. Also shown is gel-based ABPP validation of DKM 3-30 to RTN4. Pure human RTN4 protein was preincubated with DMSO or DKM for 30 min followed by IAyne labelling. Rhodamine-azide was conjugated by CuAAC and probe-labeled RTN4 was visualized by SDS/PAGE and in-gel fluorescence. (B) IsoTOP-ABPP analysis of cysteine-reactivity in pooled primary human colorectal tumors. Nine primary human colorectal tumors were pooled together and labeled with 100 or 10 μM of IAyne followed by subsequent isoTOP-ABPP analysis. Shown are ratios of heavy (100 μM) to light (10 μM) peptides. (C and D) Serum-free cell survival and proliferation (48 h) and tumor xenograft growth in SCID mice from transient siRNA or stable shRNA knockdown of RTN4 in SW620 cells. Expression was determined by qPCR. All data shown represents n = 3–6 per group. Data in (C and D) are presented as mean ± sem. Significance is expressed as *$p < 0.05$ compared to vehicle-treated or si or sh controls. Raw data for (A and B) can be found in Table S2 (ESI†).

at 100 (heavy) *versus* 10 μM (light) concentrations. Previous studies by Weerapana *et al.* have shown that hyper-reactive cysteines, which show saturated IAyne labeling at lower concentrations and thus exhibit a lower (<3) heavy to light ratio, are highly enriched in functional cysteines, compared to those sites that are not hyper-reactive that show heavy to light ratios of ~10.[8] We identify RTN4 labeling of C1101 in primary human colorectal tumors. RTN4 C1101 shows a ratio of 6.2 indicating that this cysteine is not hyper-reactive (Fig. 2B). Our data therefore shows that RTN4 is present and that C1101 within RTN4 is accessible in primary human colorectal tumors.

We confirmed the relevance of RTN4 in colorectal cancer by showing that transient or stable knockdown of RTN4 by RNA interference phenocopies the impaired survival, proliferation, and anti-tumorigenic effects observed with DKM 3-30 in SW620 colorectal cancer cells (Fig. 2C and D). To further confirm that the cell viability impairments conferred by DKM 3-30 are due to RTN4, we tested the effect of this compound in mouse embryonic fibroblasts (MEF) with or without the expression of human RTN4. Mouse Rtn4 possesses a serine instead of cysteine at the analogous site to human RTN4 (C1101). We show that DKM 3-30 does not show viability impairments in GFP-expressing MEF cells but induces apoptosis in MEF cells expressing human RTN4-GFP (Fig. S2, ESI†).

While little is known about the role of RTN4 in cancer pathogenicity, RTN4 is known to be a critical mediator of endoplasmic reticulum (ER) tubule formation.[9–11] Interestingly, Voeltz *et al.* found that tubular ER network formation in a reconstituted *in vitro* system was disrupted by thiol modifying agents and discovered that xenopus RTN4 was responsible for this action.[15] Intriguingly, one of these cysteines, C952 of xenopus RTN4,[10] corresponds to C1101 of human RTN4 identified in our study (Fig. S3, ESI†). C1101 is present in all human RTN4 isoforms, but is absent in other reticulon family members (RTN1-3) (Fig. S4, ESI†). This cysteine is positioned within a cytosolically exposed linker between two tandem hydrophobic regions (Fig. 3A), which allow RTN4 to adopt a characteristic wedge-shaped hairpin conformation required for generating highly curved membranes and tubular ER structures.[11] A solution NMR structure of a mouse RTN4 fragment revealed that this linker region forms a compact helical bundle with a portion associated with the membrane[12] and a threaded homology model of the human RTN4 linker region indicates that C1101 is present in a cytosolically accessible helix (Fig. 3A).

We postulated that covalent modification of RTN4 (C1101) by DKM 3-30 would impact the formation of ER tubular networks in cells. We attempted to analyse the effects of DKM 3-30 in SW620 colorectal cancer cells, and while the images suggest alterations in the ER morphology (Fig. S5, ESI†), the reticular nature of the ER was difficult to visualize in this cell type. Therefore, we utilized U2OS osteosarcoma cells, which are a well-established cell line for the analysis of ER morphology. As expected, control U2OS cells expressing the ER marker GFP-Sec61β displayed a highly reticular ER with clearly visible tubular ER in the cell periphery (Fig. 3B). Treatment of U2OS cells with DKM 3-30 for 8 h and 16 h resulted in a striking loss of nearly all peripheral ER tubules and an increase in ER that exhibited sheet-like morphology (Fig. 3B). To more precisely define the temporal dynamics of DKM 3-30 on ER structure, we performed time-lapse imaging of GFP-Sec61β expressing cells (Fig. 3C). In contrast to

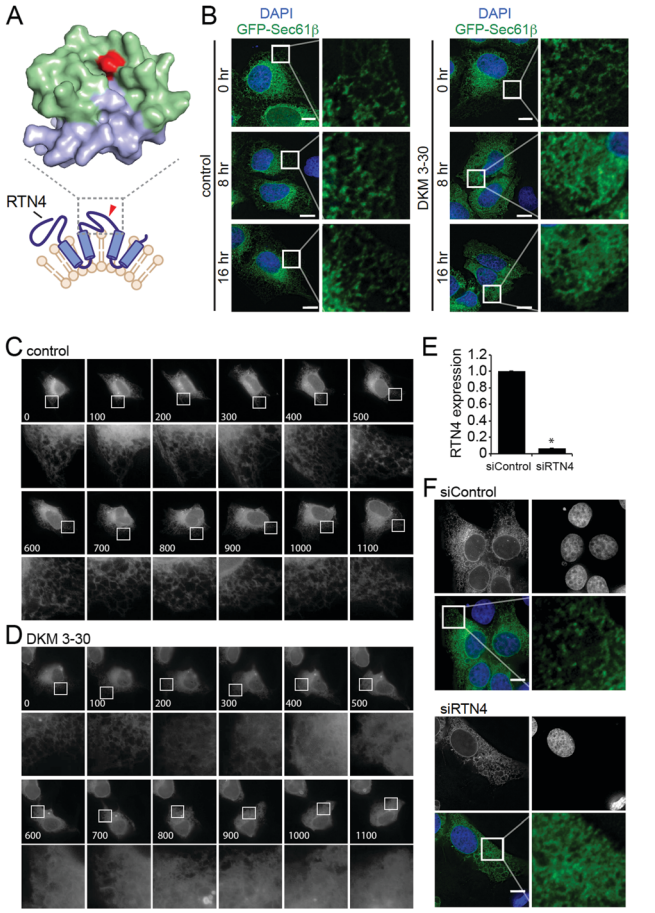

Fig. 3 DKM 3-30 disrupts the ER tubular network. (A) A schematic illustration depicts the proposed topology of Rtn4 and the position of C1101 modified by DKM 3-30 (red arrow). A homology model of human Rtn4 illustrates the membrane-associated portion (blue), the cytosolically accessible portion (green), and the position of C1101 (red). (B) U2OS cells expressing GFP-tagged Sec61β an ER marker, were treated with DKM 3-30 (50 μM) for 16 h and the ER (green) and nucleus (blue) of fixed cells visualized by fluorescence microscopy. Scale bar = 10 μm. (C and D) U2OS cells expressing GFP-tagged Sec61β were treated with vehicle (DMSO) (C) or DKM 3-30 (50 μM) (D) and ER morphology visualized by time-lapse fluorescence microscopy. Time (min) is indicated on each panel. Bottom panels indicate boxed region. (E) U2OS cells were transiently transfected with control or RTN4 siRNA and expression determined by qPCR. Data are presented as mean ± sem, $n = 3$. Significance is expressed as $*p < 0.05$. (F) U2OS cells expressing GFP-tagged Sec61β were transfected with siRNAs as in panel (D) and the ER (green) and nucleus (blue) of fixed cells visualized by fluorescence microscopy. Scale bar = 10 μm.

vehicle-treated control cells (Fig. 3C and Video S1, ESI†), treatment with DKM 3-30 resulted in the loss of peripheral ER tubules and the accumulation of sheet-like ER structures (Fig. 3D and Video S2, ESI†). The alterations in the ER morphology were evident as early as 0.5–1 h and the ER architecture became progressively more distorted, with some cells exhibiting extremely aberrant, circular ER structures (Fig. S6, ESI†). Consistent with the importance of RTN4 in ER structure, siRNA-mediated depletion of RTN4 resulted in the appearance of similarly altered ER morphologies (Fig. 3E and F). Together, these results suggest that DKM 3-30 acutely impairs RTN4 function in ER tubules formation or maintenance.

Cell division requires elaborate rearrangements in the ER and the nuclear envelope to ensure correct inheritance of DNA and

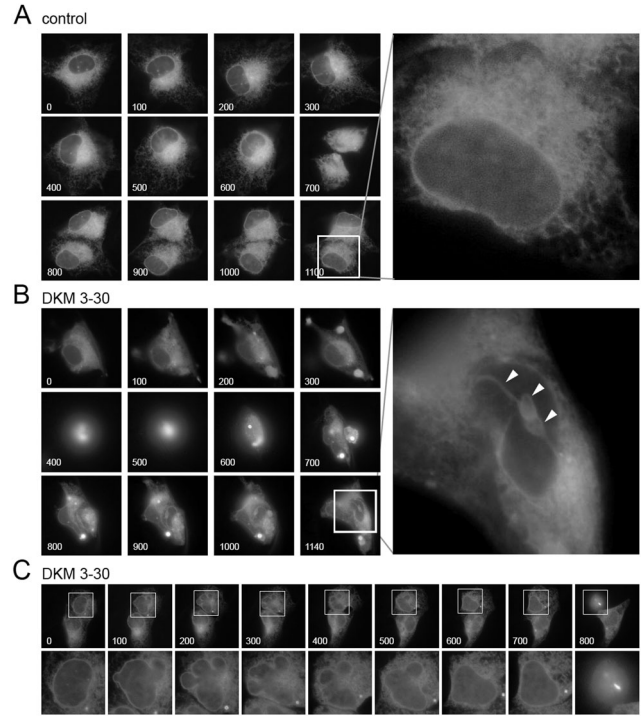

Fig. 4 DKM 3-30 disrupts nuclear envelope morphology during mitosis. (A–C) U2OS cells expressing GFP-tagged Sec61β were treated with vehicle (DMSO) or DKM 3-30 (50 μM) and ER morphology of mitotic cells visualized by time-lapse fluorescence microscopy. Time (min) is indicated on each panel. Panels (A and B) provide examples of mitotic cells. Enlarged images following mitosis show the nuclear envelope. White arrowheads indicate a GFP-Sec61β structure bisecting the nucleus of a cell incubated with DKM 3-30. (C) shows alterations in the nuclear envelope structure, followed by cell death at the 800 min time point. Bottom panels indicate boxed region.

segregation of DNA within a single nucleus.[13] During prophase the nuclear envelope retracts into the ER and then reforms during telophase. The reticulon family of proteins, and the transition between ER tubules and sheets, have been implicated in nuclear envelope assembly and disassembly during mitosis.[14–16] Time-lapse imaging of mitotic cells revealed that control cells divided rapidly (~50–60 min) (Fig. 4A and Video S3, ESI†). In contrast, DKM 3-30-treated cells exhibited prolonged mitosis (~3–4 h) (Fig. 4B and Video S4, ESI†), possibly reflecting complications in the division process. Indeed, DKM 3-30-treated cells contained aberrant nuclei that were bisected by GFP-Sec61β positive structures (Fig. 4B and Video S4, ESI†). Distortions in the nuclear envelope were also frequently observed during interphase in DKM 3-30-treated cells, including multi-lobed, cloverleaf-like nuclear envelope morphologies that often preceded cell death (Fig. 4C and Video S5, ESI†). Thus, disrupting RTN4-mediated ER remodeling may impair colorectal cancer pathogenicity by altering ER homeostasis and nuclear envelope assembly and disassembly during mitosis.

We also synthesized analogs of DKM 3-30 and showed that YP 1-46 demonstrated less displacement of IAyne labelling of RTN4, whereas AMR 1-125 exhibited ~7-fold improved potency compared to DKM 3-30. We further showed that AMR 1-125, but not YP 1-46, impaired cell survival in U2OS and SW620 cells and ER morphology in U2OS cells (Fig. 5A–C and Fig. S7, ESI†).

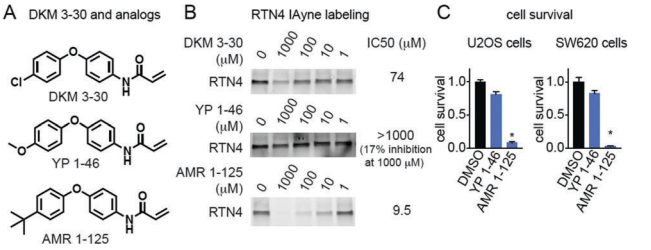

Fig. 5 DKM 3-30 and analogs. (A) Structures of DKM 3-30 and analogs. (B) Gel-based ABPP analysis showing competition side-by-side competition studies of DKM 3-30, YP 1-46, and AMR 1-125 against IA-rhodamine labelling of pure human RTN4. Shown are the 50% inhibitory concentration (IC50) values for each compound. (C) Serum-free cell survival of U2OS (48 h) or SW620 (24 h) cells treated with DMSO vehicle or each compound (50 μM). Data in (C) are presented as mean ± sem. Significance is expressed as $*p < 0.001$ compared to vehicle-treated controls.

In summary, we identify RTN4 as a novel colorectal cancer therapeutic target, and reveal a unique druggable hotspot within this classically undruggable protein, which can be targeted by cysteine-reactive ligands such as DKM 3-30 to impair ER and nuclear envelope morphology and colorectal cancer pathogenicity. Overall, we highlight the utility of coupling the screening of covalent ligand libraries with isoTOP-ABPP for mining the proteome for novel druggable nodes that can be targeted for cancer therapy.

This work was supported by grants from the National Institutes of Health (R01CA172667 for DKN, LAB, TRH, DKM, YP, R01GM112948 for JAO, TBN), American Cancer Society Research Scholar Award (RSG14-242-01-TBE for DKN, LAB, TRH, DKM).

Notes and references

1 N. M. Gangadhar and B. R. Stockwell, *Curr. Opin. Chem. Biol.*, 2007, **11**, 83–87.
2 I. Smukste and B. R. Stockwell, *Annu. Rev. Genomics Hum. Genet.*, 2005, **6**, 261–286.
3 E. Weerapana, C. Wang, G. M. Simon, F. Richter, S. Khare, M. B. D. Dillon, D. A. Bachovchin, K. Mowen, D. Baker and B. F. Cravatt, *Nature*, 2010, **468**, 790–795.
4 K. M. Backus, B. E. Correia, K. M. Lum, S. Forli, B. D. Horning, G. E. González-Páez, S. Chatterjee, B. R. Lanning, J. R. Teijaro, A. J. Olson, D. W. Wolan and B. F. Cravatt, *Nature*, 2016, **534**, 570–574.
5 C. Wang, E. Weerapana, M. M. Blewett and B. F. Cravatt, *Nat. Methods*, 2014, **11**, 79–85.
6 F. N. B. Edfeldt, R. H. A. Folmer and A. L. Breeze, *Drug Discovery Today*, 2011, **16**, 284–287.
7 V. V. Rostovtsev, L. G. Green, V. V. Fokin and K. B. Sharpless, *Angew. Chem., Int. Ed. Engl.*, 2002, **41**, 2596–2599.
8 E. Weerapana, G. M. Simon and B. F. Cravatt, *Nat. Chem. Biol.*, 2008, **4**, 405–407.
9 L. Jozsef, K. Tashiro, A. Kuo, E. J. Park, A. Skoura, S. Albinsson, F. Rivera-Molina, K. D. Harrison, Y. Iwakiri, D. Toomre and W. C. Sessa, *J. Biol. Chem.*, 2014, **289**, 9380–9395.
10 G. K. Voeltz, W. A. Prinz, Y. Shibata, J. M. Rist and T. A. Rapoport, *Cell*, 2006, **124**, 573–586.
11 Y. Shibata, J. Hu, M. M. Kozlov and T. A. Rapoport, *Annu. Rev. Cell Dev. Biol.*, 2009, **25**, 329–354.
12 S. V. Vasudevan, J. Schulz, C. Zhou and M. J. Cocco, *Proc. Natl. Acad. Sci. U. S. A.*, 2010, **107**, 6847–6851.
13 S. Güttinger, E. Laurell and U. Kutay, *Nat. Rev. Mol. Cell Biol.*, 2009, **10**, 178–191.
14 D. J. Anderson and M. W. Hetzer, *J. Cell Biol.*, 2008, **182**, 911–924.
15 E. Kiseleva, K. N. Morozova, G. K. Voeltz, T. D. Allen and M. W. Goldberg, *J. Struct. Biol.*, 2007, **160**, 224–235.
16 A. Audhya, A. Desai and K. Oegema, *J. Cell Biol.*, 2007, **178**, 43–56.

